Exciton–Dissociation and Charge–Recombination Processes in Pentacene/C-60 Solar Cells: Theoretical Insight into the Impact of Interface Geometry

3 AUTHORS, INCLUDING:

Yuanping Yi
Chinese Academy of Sciences
82 PUBLICATIONS **1,567** CITATIONS

SEE PROFILE

Veaceslav Coropceanu
Georgia Institute of Technology
125 PUBLICATIONS **7,426** CITATIONS

SEE PROFILE

Exciton-Dissociation and Charge-Recombination Processes in Pentacene/C_{60} Solar Cells: Theoretical Insight into the Impact of Interface Geometry

Yuanping Yi, Veaceslav Coropceanu,* and Jean-Luc Brédas*

School of Chemistry and Biochemistry and Center for Organic Photonics and Electronics, Georgia Institute of Technology, Atlanta, Georgia 30332-0400

Received July 17, 2009; E-mail: coropceanu@gatech.edu; jean-luc.bredas@chemistry.gatech.edu

Abstract: The exciton-dissociation and charge-recombination processes in organic solar cells based on pentacene/C_{60} heterojunctions are investigated by means of quantum-mechanical calculations. The electronic couplings and the rates of exciton dissociation and charge recombination have been evaluated for several geometrical configurations of the pentacene/C_{60} complex, which are relevant to bilayer and bulk heterojunctions. The results suggest that, irrespective of the actual pentacene−fullerene orientation, both pentacene-based and C_{60}-based excitons are able to dissociate efficiently. Also, in the case of parallel configurations of the molecules at the pentacene/C_{60} interface, the decay of the lowest charge-transfer state to the ground state is calculated to be very fast; as a result, it can compete with the dissociation process into mobile charge carriers. Since parallel configurations are expected to be found more frequently in bulk heterojunctions than in bilayer heterojunctions, the performance of pentacene/C_{60} bulk-heterojunction solar cells is likely to be more affected by charge recombination than that of bilayer devices.

1. Introduction

Organic solar cells are currently attracting significant interest due to their potential advantages in terms of low cost, flexibility, large-area capability, and easy processing.[1−10] The active layers typically consist of two components, an electron-donor (D) and an electron-acceptor (A) material, assembled either into a bilayer structure or in the form of a blend. In both instances, the mechanism of photocurrent production is based on initial generation of excitons by sunlight absorption, followed by diffusion of these excitons to the D/A interface and their dissociation into separated charge carriers (electrons and holes), which migrate to and are collected at the electrodes.

The optimization of organic solar cells requires a fine balancing act. It involves finding the optimal compromise among a combination of material characteristics that sometimes happen to work in opposite directions. As an example, the local D/A interface geometry or morphology can have a positive impact on both exciton dissociation (which produces the photocurrent and needs to be maximized) and the recombination of charge-transfer states formed after exciton dissociation (which decreases the photocurrent and needs to be minimized), as well as on the magnitude of the reverse saturation current in the dark (which needs to be minimized to increase the open-circuit voltage).[11−13]

Here, we investigate the charge-transfer (CT) and charge-recombination (CR) processes in organic solar cells based on pentacene/fullerene (P/C_{60}) heterojunctions. Recently, the P/C_{60} system has received much attention as a model for small-molecule organic photovoltaic (OPV) cells.[14−27] The most

(1) Scharber, M. C.; Mühlbacher, D.; Koppe, M.; Denk, P.; Waldauf, C.; Heeger, A. J.; Brabec, C. J. *Adv. Mater.* **2006**, *18*, 789–794.
(2) Gunes, S.; Neugebauer, H.; Sariciftci, N. S. *Chem. Rev.* **2007**, *107*, 1324–1338.
(3) Kroon, R.; Lenes, M.; Hummelen, J. C.; Blom, P. W. M.; De Boer, B. *Polym. Rev.* **2008**, *48*, 531–582.
(4) Mayer, A. C.; Scully, S. R.; Hardin, B. E.; Rowell, M. W.; McGehee, M. D. *Mater. Today* **2007**, *10*, 28–33.
(5) Kippelen, B.; Brédas, J. L. *Energy Environ. Sci.* **2009**, *2*, 251–261.
(6) Thompson, B. C.; Frechet, J. M. J. *Angew. Chem., Int. Ed.* **2008**, *47*, 58–77.
(7) Rand, B. P.; Burk, D. P.; Forrest, S. R. *Phys. Rev. B* **2007**, *75*, 659–676.
(8) Riede, M.; Mueller, T.; Tress, W.; Schueppel, R.; Leo, K. *Nanotechnology* **2008**, *19*, 424001.
(9) Lloyd, M. T.; Anthony, J. E.; Malliaras, G. G. *Mater. Today* **2007**, *10*, 34–41.
(10) Brédas, J.-L.; Norton, J. E.; Cornil, J.; Coropceanu, V. *Acc. Chem. Res.*, published ASAP online Aug 4, 2009 (http://dx.doi.org/10.1021/ar900099h).

(11) Potscavage, W. J.; Yoo, S.; Kippelen, B. *Appl. Phys. Lett.* **2008**, *93*, 193308.
(12) Li, N.; Lassiter, B. E.; Lunt, R. R.; Wei, G.; Forrest, S. R. *Appl. Phys. Lett.* **2009**, *94*, 023307.
(13) Perez, M. D.; Borek, C.; Forrest, S. R.; Thompson, M. E. *J. Am. Chem. Soc.* **2009**, *131*, 9281–9286.
(14) Yoo, S.; Domercq, B.; Kippelen, B. *Appl. Phys. Lett.* **2004**, *85*, 5427–5429.
(15) Yoo, S.; Potscavage, W. J.; Domercq, B.; Han, S.-H.; Li, T.-D.; Jones, S. C.; Szoszkiewicz, R.; Levi, D.; Riedo, E.; Marder, S. R.; Kippelen, B. *Solid-State Electron.* **2007**, *51*, 1367–1375.
(16) Yoo, S.; Domercq, B.; Kippelen, B. *J. Appl. Phys.* **2005**, *97*, 103706.
(17) Palilis, L. C.; Lane, P. A.; Kushto, G. P.; Purushothaman, B.; Anthony, J. E.; Kafafi, Z. H. *Org. Electron.* **2008**, *9*, 747–752.
(18) Sullivan, P.; Jones, T. S. *Org. Electron.* **2008**, *9*, 656–660.
(19) Nanditha, D. M.; Dissanayake, M.; Hatton, R. A.; Curry, R. J.; Silva, S. R. P. *Appl. Phys. Lett.* **2007**, *90*, 113505.
(20) Pandey, A. K.; Shaw, P. E.; Samuel, I. D. W.; Nunzi, J. M. *Appl. Phys. Lett.* **2009**, *94*, 103303.
(21) Yang, J.; Nguyen, T. Q. *Org. Electron.* **2007**, *8*, 566–574.
(22) Salzmann, I.; Duhm, S.; Opitz, R.; Johnson, R. L.; Rabe, J. P.; Koch, N. *J. Appl. Phys.* **2008**, *104*, 114518.
(23) Cheyns, D.; Gommans, H.; Odijk, M.; Poortmans, J.; Heremans, P. *Sol. Energy Mater.* **2007**, *91*, 399–404.
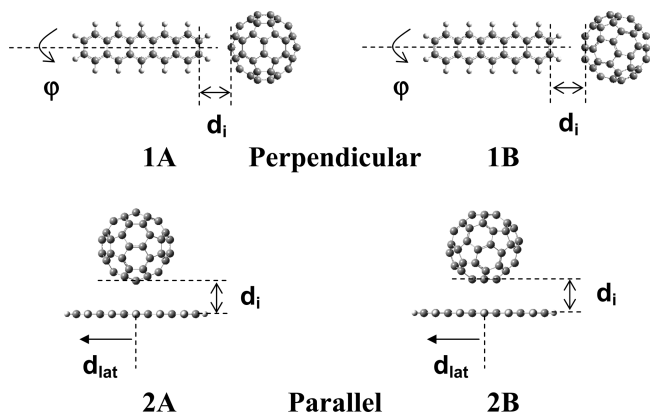(24) Pandey, A. K.; Nunzi, J.-M. *Appl. Phys. Lett.* **2006**, *89*, 213506.

Figure 1. Illustration of the pentacene/C_{60} configurations used in the calculations, where the intermolecular distance d_i, the lateral displacement d_{lat}, and the rotation angle of pentacene φ are varied. In configuration 1A or 1B [2A or 2B], the pentacene molecule is perpendicular [parallel] to a carbon−carbon double bond or hexagon of C_{60}.

investigated P/C_{60} OPV devices are based on a bilayer heterojunction configuration. Device characterizations and atomic force microscopy measurements underline that films with a more regular crystalline structure lead to higher device performance.[21] Ordered pentacene films usually grow with the pentacene long-axis oriented perpendicular to the substrate (*c*-axis oriented crystal), for instance, indium−tin oxide glass (ITO)/poly(3,4-ethylenedioxythiophene):poly(styrenesulfonate) (PEDOT:PSS).[21] This molecular orientation is in fact less favorable for hole transport since intermolecular electronic couplings are weaker along the *c*-axis.[28] In addition, in a bilayer P/C_{60} heterojunction, a significant number of P/C_{60} pairs find themselves in a perpendicular orientation (Figure 1); as will be shown below, this intermolecular orientation is less favorable for efficient exciton dissociation. Therefore, it can be surprising that P/C_{60} bilayer OPV devices present a reasonably high power conversion efficiency (PCE) of about 2% (under 1 sun AM1.5G illumination).[14,15]

More recently, solar cells based on P/C_{60} bulk heterojunctions were also studied.[22,29] The main advantage of a bulk heterojunction over a planar bilayer heterojunction is that excitons can dissociate throughout the bulk; i.e., a bulk heterojunction allows for a larger D/A interfacial area.[30] In the case of P/C_{60} bulk heterojunctions, a significant number of P/C_{60} pairs can be expected to be in a parallel orientation (Figure 1), a configuration more suitable for strong electronic coupling between the pentacene and C_{60} electronic states and, consequently, for efficient exciton dissociation. However, although devices based on P/C_{60} bulk heterojunctions yield a slightly higher open-circuit voltage than bilayer devices, the short-circuit current density and the overall PCE of bulk-heterojunction devices are about 6 times lower than those of planar-heterojunction devices.[22,29] It was suggested that this difference in

performance could be due to the substantial phase separation observed in P/C_{60} bulk heterojunctions leading to a large size of the crystalline domains, high surface roughness, and possible electrical shorts between electrodes.[22,29]

It is our primary goal in this contribution to investigate the role of the P/C_{60} interface geometry on the efficiency of both exciton-dissociation and charge-recombination processes and to rationalize some of the differences in performance between the bilayer- and bulk-heterojunction architectures. Using a methodology that we recently developed,[31] we investigate these processes for the configurations illustrated in Figure 1.

2. Methodology

The geometry optimizations of the isolated pentacene and fullerene (C_{60}) molecules were performed at the density functional theory (DFT) B3LYP level using the 6-31G(d,p) basis set as implemented in the Gaussian03 package.[32] Based on the DFT-optimized geometries, the excited-state energies were evaluated both at the time-dependent (TD) DFT/B3LYP 6-31G(d,p) level of theory and by means of the intermediate neglect of differential overlap (INDO) Hamiltonian[33] coupled to a single configuration interaction (SCI) scheme. To analyze the electronic couplings (V_{ab}) between the lowest intramolecular (local) singlet/triplet states and the lowest CT states, we used the approach recently developed in our group; the methodology is based on the construction of local ground and excited states (Ψ_a^{LE}) and CT states (Ψ_b^{CT}) as spin-adapted antisymmetrized products of the isolated donor (ψ_i^D) and acceptor (ψ_j^A) wave functions:[31]

$$V_{ab} = \langle \Psi_a^{LE} | H | \Psi_b^{CT} \rangle \qquad (1)$$

$$\Psi_{ij}^{LE}(SM) = \sum_{M_i M_j} C_{S_i M_i S_j M_j}^{SM} |\psi_i^D(S_i M_i)\psi_j^A(S_j M_j)| \qquad (2)$$

$$\Psi_{km}^{CT}(SM) = \sum_{M_k M_m} C_{S_k M_k S_m M_m}^{SM} |\psi_k^{D+}(S_k M_k)\psi_m^{A-}(S_m M_m)| \qquad (3)$$

Here, **S** and **M** denote the total spin and spin projection for the donor−acceptor complex; S_n and M_n are the corresponding variables for the isolated donor and acceptor molecules (D and A) and their oxidized and reduced states, D^+ and A^-. The $C_{S_i M_i S_j M_j}^{SM}$ terms represent the Clebsch−Gordan (CG) coefficients, which ensure that the linear combination of the isolated wave function products is the eigenstate of the total spin. These calculations were performed at the INDO level of theory with the Mataga−Nishimoto potential to describe the Coulomb repulsion term.[34,35] All the π-type molecular orbitals (MOs) were taken into account to construct the CI active space for pentacene (11 occupied and 11 unoccupied MOs) and C_{60} (30 occupied and 30 unoccupied MOs). Due to the three-fold degeneracy of the LUMO in C_{60}, three negatively charged configurations were used as the reference determinants to calculate the anionic states for C_{60}.

The rates of exciton dissociation and charge recombination were evaluated using the Marcus semiclassical model:[36]

$$k_{ab} = V_{ab}^2 \sqrt{\frac{\pi}{\lambda k_B T \hbar^2}} \exp[-(\Delta G + \lambda)^2 / 4\lambda k_B T] \qquad (4)$$

(25) Dissanayake, D. M. N. M.; Adikaari, A. A. D. T.; Curry, R. J.; Hatton, R. A.; Silva, S. R. P. *Appl. Phys. Lett.* **2007**, *90*, 253502.

(26) Kinoshita, Y.; Hasobe, T.; Murata, H. *Appl. Phys. Lett.* **2007**, *91*, 083518.

(27) Tseng, C.-T.; Cheng, Y.-H.; Lee, M.-C. M.; Han, C.-C.; Cheng, C.-H.; Tao, Y.-T. *Appl. Phys. Lett.* **2007**, *91*, 233510.

(28) Coropceanu, V.; Cornil, J.; da Silva Filho, D. A.; Olivier, Y.; Silbey, R.; Brédas, J. L. *Chem. Rev.* **2007**, *107*, 926–952.

(29) Zheng, Y.; Pregler, S. K.; Myers, J. D.; Ouyang, J. M.; Sinnott, S. B.; Xue, J. G. *J. Vac. Sci. Technol. B* **2009**, *27*, 169–179.

(30) Yu, G.; Gao, J.; Hummelen, J. C.; Wudl, F.; Heeger, A. J. *Science* **1995**, *270*, 1789–1791.

(31) Kawatsu, T.; Coropceanu, V.; Ye, A.; Brédas, J. L. *J. Phys. Chem. C* **2008**, *112*, 3429–3433.

(32) Frisch, M. J.; et al. *Gaussian 03*; Gaussian, Inc.: Pittsburgh, PA, 2003.

(33) Ridley, J.; Zerner, M. *Theor. Chim. Acta* **1973**, *32*, 111–134.

(34) Mataga, N.; Nishimoto, K. *Z. Phys. Chem.* **1957**, *12*, 35.

(35) Mataga, N.; Nishimoto, K. *Z. Phys. Chem.* **1957**, *13*, 140.

(36) Marcus, R. A. *Rev. Mod. Phys.* **1993**, *65*, 599–610.

Table 1. Excitation Energies for the Lowest Singlet and Triplet Excited States and Ionization Energies in Pentacene and C$_{60}$ (in eV)

|	C$_{60}$			pentacene		
state	INDO	DFT	state	INDO	DFT
$^1T_{1g}$	2.24	2.11	$^1B_{1u}$	2.62	1.95
$^1T_{2g}$	2.26	2.11	$^3B_{1u}$	0.41	0.59
^1G_g	2.28	2.10			
$^3T_{2g}$	1.19	1.60			
EA ($^2T_{1u}$)	−1.48	−2.0/−2.10^a	IP ($^2B_{2g}$)	5.95	5.95/5.85^a

^{a} Based on the optimized geometry of the charged state (adiabatic values).

Here, λ is the reorganization energy, ΔG the Gibbs free energy (driving force), k_B the Boltzmann constant, and T the temperature.

3. Results and Discussion

3.1. Molecular States. The calculated excitation and ionization energies are given in Table 1. The C$_{60}$ molecule belongs to the icosahedral (I_h) point group; its electronic ground state presents A_g symmetry. The lowest four singlet excited states ($^1T_{1g}$, $^1T_{2g}$, ^1G_g, ^1H_g) originate from a 15-fold degenerate HOMO (h$_u$)−LUMO (t$_{1u}$) configuration. As a result of such a symmetry, one-photon optical transitions from the ground state to these excited states are forbidden and can take place only by means of vibronic coupling.[37] As can be seen from Table 1, the $^1T_{1g}$, $^1T_{2g}$, and ^1G_g states are practically degenerate; it was suggested that the fluorescence spectra observed in inert matrices made of noble gas atoms represent a mixing of contributions from these three states.[38,39] The analysis of the fluorescence spectra suggests that the electronic origin (0−0 transition) of the lowest singlet state S$_1$ of C$_{60}$ in the gas phase is about 1.94 eV.[37] As can be seen from Table 1, both the TD-DFT and INDO estimates of the S$_1$ energy, though somewhat higher, agree very well with the experimental value. In the solid state, the S$_1$ energy in C$_{60}$ is estimated to lie about 1.70 eV above the ground state.[40] The lowest triplet state T$_1$ of C$_{60}$ belongs to the T$_{2g}$ irreducible representation; according to optical measurements, it has an energy of *ca.* 1.55 eV.[37] The TD-DFT estimate is in excellent agreement with experiment, while the INDO calculations underestimate the T$_1$ energy.

The closed-shell ground state of pentacene belongs to the A_g irreducible representation of the D_{2h} molecular point group of symmetry. The energy of the first excited singlet state ($^1B_{1u}$) measured from the absorption spectrum in a dichlorobenzene solution is 2.10 eV[41] and red-shifts to 1.85 eV in the solid state.[42,43] The lowest triplet state ($^3B_{1u}$) is located about 0.86 eV above the ground state.[44] As can be seen from Table 1, the TD-DFT estimates (obtained for an isolated molecule) of S$_1$ and T$_1$ energies compare well with experiment, while again the
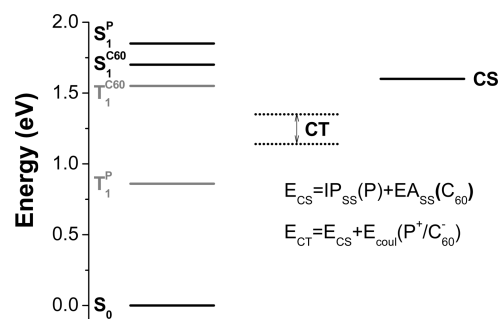
Figure 2. Energy diagram for the monomer and charge-transfer states used in the calculations of the exciton-dissociation and charge-recombination rates.

INDO calculations overestimate the S$_1$ energy and underestimate the T$_1$ energy.

The lowest diabatic CT state (CT$_0$) is described as the direct product of the ground state of the radical cation of pentacene ($^2B_{2g}$) and the ground state of the radical anion of C$_{60}$ ($^2T_{1u}$). The energies of these two states can be obtained experimentally by means of photoelectron and inverse photoemission spectroscopies by measuring the first ionization potential (IP) of pentacene and the electron affinity (EA) of C$_{60}$. In the gas phase, IP$_{gas}$(P) = 6.59 eV[45] and EA$_{gas}$(C$_{60}$) = −2.68 eV.[46] In the solid state, these quantities are substantially modified due to polarization contributions: IP$_{ss}$(P) = 5.1 eV[47] and EA$_{ss}$(C$_{60}$) = −3.5 eV.[48] The lowest excited CT states (CT$_1$, CT$_2$) arise from the first excited state of the radical anion of C$_{60}$ and the cation of pentacene; from electronic absorption spectra, these two states are located 1.15 eV[49,50] and 1.31 eV,[51] respectively, above the corresponding ground states of the charged species. Because the CT$_1$ and CT$_2$ states are much higher in energy than the CT$_0$ state, the latter state is expected to play the most significant role in the exciton-dissociation process, as detailed below. In the calculations of the exciton-dissociation and charge-recombination rates, we have made use of the experimental values for the energies, as estimated in the solid state; the related energy diagram is shown in Figure 2.

3.2. Electronic Couplings. The ground, local-excited, and CT states of the P/C$_{60}$ complex obtained from a ψ_i^P state of pentacene and a $\psi_j^{C_{60}}$ state of C$_{60}$ are denoted here as $\psi_i^P \otimes \psi_j^{C_{60}}$; for instance, the CT$_0$ state is represented as $^2B_{2g}{}^{P+} \otimes {}^2T_{1u}{}^{C_{60}-}$. As discussed above, the CT$_0$ state as well as local excited states of C$_{60}$ are orbitally degenerate. Therefore, for a full characterization of the electronic interaction between a CT state and a local state, it is necessary to provide $g_{CT} \otimes g_L$ matrix elements, where g_{CT} and g_L denote the respective multiplicity of the involved states. We note, however, that CT and CR rates according to eq 4 depend on an effective electronic coupling V_{eff} that accounts for all $g_{CT} \otimes g_L$ elements:

(37) Orlandi, G.; Negri, F. *Photochem. Photobiol. Sci.* **2002**, *1*, 289–308.
(38) Sassara, A.; Zerza, G.; Chergui, M. *J. Phys. B: At., Mol. Opt. Phys.* **1996**, *29*, 4997–5013.
(39) Sassara, A.; Zerza, G.; Chergui, M.; Negri, F.; Orlandi, G. *J. Chem. Phys.* **1997**, *107*, 8731–8741.
(40) Akimoto, I.; Ashida, M.; Kan'no, K. *Chem. Phys. Lett.* **1998**, *292*, 561–566.
(41) Sakamoto, Y.; Suzuki, T.; Kobayashi, M.; Gao, Y.; Fukai, Y.; Inoue, Y.; Sato, F.; Tokito, S. *J. Am. Chem. Soc.* **2004**, *126*, 8138–8140.
(42) Jundt, C.; Klein, G.; Sipp, B.; Lemoigne, J.; Joucla, M.; Villaeys, A. A. *Chem. Phys. Lett.* **1995**, *241*, 84–88.
(43) Faltermeier, D.; Gompf, B.; Dressel, M.; Tripathi, A. K.; Pflaum, J. *Phys. Rev. B* **2006**, *74*, 125416.
(44) Burgos, J.; Pope, M; Swenberg, Ch. E.; Alfano, R. R. *Phys. Stat. Solidi (b)* **1977**, *83*, 249–256.

(45) Gruhn, N. E.; da Silva, D. A.; Bill, T. G.; Malagoli, M.; Coropceanu, V.; Kahn, A.; Bredas, J. L. *J. Am. Chem. Soc.* **2002**, *124*, 7918–7919.
(46) Wang, X. B.; Woo, H. K.; Wang, L. S. *J. Chem. Phys.* **2005**, *123*, 051106.
(47) Hwang, J.; Wan, A.; Kahn, A. *Mater. Sci. Eng. Rep.* **2009**, *64*, 1–31.
(48) Schwedhelm, R.; Kipp, L.; Dallmeyer, A.; Skibowski, M. *Phys. Rev. B* **1998**, *58*, 13176–13180.
(49) Kato, T.; Kodama, T.; Shida, T.; Nakagawa, T.; Matsui, Y.; Suzuki, S.; Shiromaru, H.; Yamauchi, K.; Achiba, Y. *Chem. Phys. Lett.* **1991**, *180*, 446–450.
(50) Kato, T.; Kodama, T.; Shida, T. *Chem. Phys. Lett.* **1993**, *205*, 405–409.
(51) Szczepanski, J.; Wehlburg, C.; Vala, M. *Chem. Phys. Lett.* **1995**, *232*, 221–228.

$$V_{\text{eff};ab}^2 = \frac{1}{g_a} \sum_{ij} (\Psi_{ai}|H|\Psi_{bj})^2 \qquad (5)$$

Interestingly, the calculations show that the effective electronic couplings between the CT_0 and any of the T_{1g}, T_{2g}, and G_g states that contribute to the formation of the S_1 state in C_{60} are all very similar [see Table S1 in the Supporting Information (SI)]. Therefore, it can be assumed without any loss of generality that the S_1 state of C_{60} arises simply from one of these three terms; we chose here to deal with state $^1T_{1g}$.

The calculated electronic couplings involving CT_0 for the perpendicular and parallel configurations of the P/C_{60} complex are given in Figures 3 and 4, respectively. The results confirm that the electronic couplings significantly depend on both intermolecular distance and relative molecular orientations. For the same intermolecular distance (d_i), the electronic couplings obtained in the case of parallel configurations are significantly larger than in the case of perpendicular orientations; for the intermolecular distance corresponding to the sum of the van der Waals radii of the closest atoms of pentacene and C_{60} molecules (which represents the smallest intermolecular distance considered here), the electronic coupling can be as large as 600 cm^{-1}.

Except for the case of orientation 1A (pentacene perpendicular to a C=C edge, see Figure 1) where, due to symmetry reasons, there is no interaction between the ground state and the CT_0 state, the respective coupling is significant in all other cases. In the case of perpendicular orientations, there is also a significant coupling between the CT_0 state and the first excited state of pentacene. For parallel orientations, the first excited states of both pentacene and C_{60} exhibit similar couplings to the CT_0 state.

The electronic couplings for all states show the expected exponential dependence on intermolecular distance d_i. The oscillatory dependence of V_{eff} on lateral distance is due to the modulation of the bonding/antibonding pattern of the involved molecular orbitals. A similar oscillatory dependence was found previously for electronic couplings related to charge transport in organic systems.[52,53]

The electronic couplings between the lowest local-excited states and the lowest excited CT states (CT_1 and CT_2) show trends very similar to those derived for CT_0 (see Figures S1–S4 in SI for more detail).

3.3. Exciton-Dissociation and Charge-Recombination Rates. In order to evaluate the CT and CR rates according to eq 4, in addition to the electronic couplings, we also need to estimate the Gibbs free energy, ΔG, and the reorganization energy, λ. ΔG is approximated here as the energy difference between the involved local and CT states of the P/C_{60} complex. Since experimental data are available, the energies of the local excited states of the P/C_{60} complex are taken to correspond to the energies of the related intramolecular states measured in the solid state. The energy of the CT_0 state (in eV) is estimated as

$$E_{CT} = IP_{SS}(P) + EA_{SS}(C_{60}) + E_{Coul}(P^+/C_{60}^-)$$
$$= 1.6 + E_{Coul}(P^+/C_{60}^-) \qquad (6)$$

$E_{Coul}(P^+/C_{60}^-)$ represents the Coulomb interaction energy between the cation of pentacene and anion of C_{60} and is computed as

$$E_{Coul} = \sum_{g \in P, h \in C_{60}} (q_g q_h / \varepsilon r_{gh}) \qquad (7)$$

where q_g and q_h are the partial charges (obtained via an INDO Mulliken population analysis) on atoms g and h of the pentacene cation and the C_{60} anion, respectively, r_{gh} is the distance between these atoms, and ε is the dielectric constant; here, we have taken $\varepsilon = 4$, which represents an average between the typical values reported for C_{60} and pentacene.[54,55]

The results for E_{Coul} are shown in Figure 5. The electrostatic energy leads to a significant stabilization of the CT states, by up to 0.3 and 0.5 eV in the case of perpendicular and parallel orientations, respectively. The increase of d_i [d_{lat}] from 3.5 to 6 Å [0 to 12 Å] (the upper limit is where the electronic coupling vanishes) results in a decrease in the absolute value of E_{Coul} by about 0.1 eV [0.2 eV].

In eq 6, for simplicity, we assumed that the electronic polarization contribution to the CT state is equal to that in bulk materials. Clearly, a more refined approach that considers the dependence of electronic polarization energy and effective local dielectric constant on intermolecular distance and heterojunction morphology is needed.[56] It is, however, important to note that photoelectron spectroscopy measurements show that the relative positions of the frontier electronic states of pentacene and C_{60} in bilayer and bulk heterojunctions are very similar.[22] These findings suggest that, at least in the present case, the heterojunction morphology has only a small effect on the electronic polarization energy. We also point to the fact that the expected increase in electronic polarization stabilization with the intermolecular distance between the cation of pentacene and anion of C_{60} should go in parallel with an increase in the effective local dielectric constant, which in turn will reduce the electrostatic energy. Since these two contributions act in opposite directions and tend to compensate one another, eq 6, in spite of the crude approximations that are made, is expected to provide a reasonable description of the dependence of the CT energy on intermolecular distance.

The energies of the lowest excited CT states can be estimated in a similar way. Our calculations show that the Coulomb energy for CT_1 and CT_2 is similar to that of CT_0; as a result, these two states are located above the lowest local-excited states for all P/C_{60} configurations we considered. Therefore, we will restrict our discussion of the CT and CR processes to those involving the CT_0 state.

We now turn to the reorganization energy, which consists of intra- and intermolecular contributions; the former reflects changes in the geometry of individual molecules and the latter in the polarization of the surrounding molecules upon going from the neutral to the charged state and vice versa. The intramolecular reorganization energy, λ_i, can be easily estimated from adiabatic potential energy surfaces of the molecular states involved in the considered electron-transfer process. For instance, λ_i for the transition from the ground state of the P/C_{60}

(52) Brédas, J. L.; Beljonne, D.; Coropceanu, V.; Cornil, J. *Chem. Rev.* **2004**, *104*, 4971–5003.

(53) Brédas, J. L.; Calbert, J. P.; da Silva, D. A.; Cornil, J. *Proc. Natl. Acad. Sci. U.S.A.* **2002**, *99*, 5804–5809.

(54) Ruoff, R. S.; Tse, D. S.; Malhotra, R.; Lorents, D. C. *J. Phys. Chem.* **1993**, *97*, 3379–3383.

(55) Dressel, M.; Gompf, B.; Faltermeier, D.; Tripathi, A. K.; Pflaum, J.; Schubert, M. *Opt. Express* **2008**, *16*, 19770–19778.

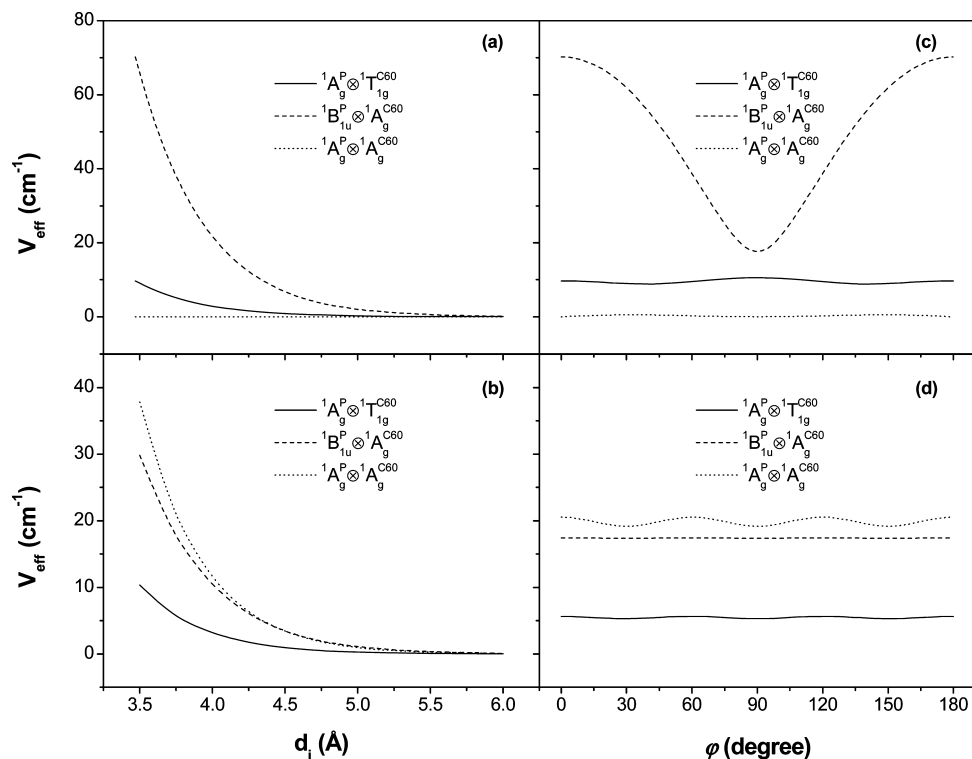(56) Verlaak, S.; Beljonne, D.; Cheyns, D.; Rolin, C.; Linares, M.; Castet, F.; Cornil, J.; Heremans, P., submitted.

Figure 3. Electronic couplings of the local-excited singlet states ($^1A_g{}^P \otimes {}^1T_{1g}{}^{C_{60}}$ and $^1B_{1u}{}^P \otimes {}^1A_g{}^{C_{60}}$) and of the ground state ($^1A_g{}^P \otimes {}^1A_g{}^{C_{60}}$) with the lowest CT state ($^2B_{2g}{}^{P+} \otimes {}^2T_{1u}{}^{C_{60}-}$) for perpendicular orientations 1A and 1B of Figure 1, as a function of intermolecular distance (plots a and b, respectively) and as a function of the rotation angle of pentacene with d_i = 3.47 and 3.76 Å for orientations 1A and 1B (plots c and d), respectively.
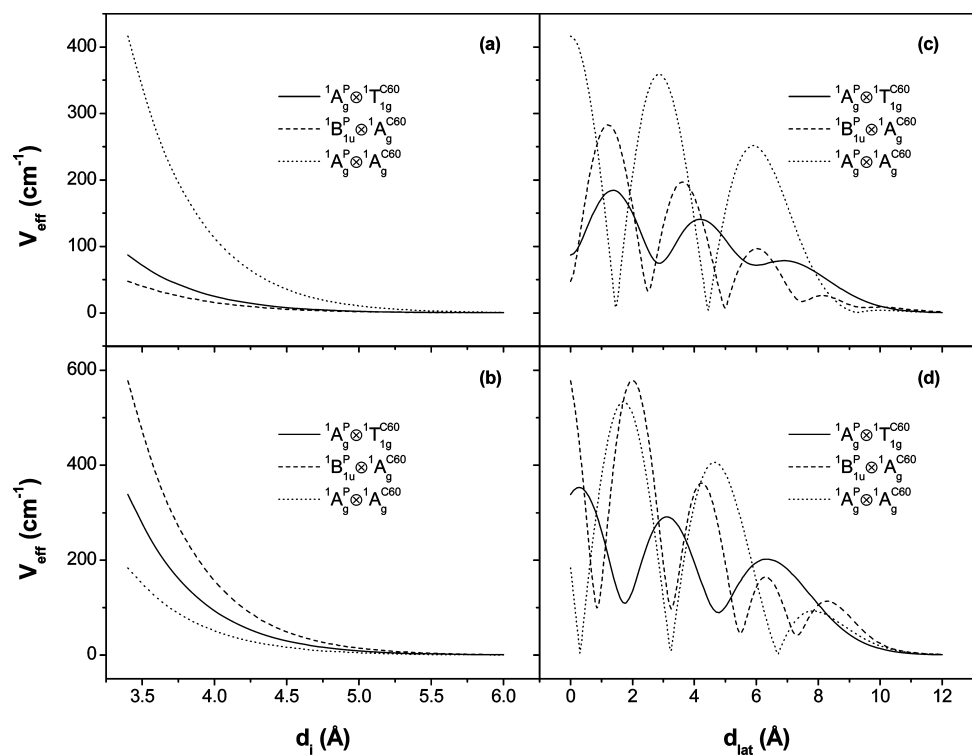
Figure 4. Electronic couplings of the local-excited singlet states ($^1A_g{}^P \otimes {}^1T_{1\ g}{}^{C_{60}}$ and $^1B_{1u}{}^P \otimes {}^1A_g{}^{C_{60}}$) and of the ground state ($^1A_g{}^P \otimes {}^1A_g{}^{C_{60}}$) with the lowest CT state ($^2B_{2\ g}{}^{P+} \otimes {}^2T_{1u}{}^{C_{60}-}$) for parallel orientations 2A and 2B of Figure 1, as a function of intermolecular distance (plots a and b, respectively) and as a function of lateral displacement with d_i set at 3.5 Å (plots c and d, respectively).

complex to its lowest CT state is equal to the sum of the relaxation energies upon oxidation of pentacene and reduction of C$_{60}$. DFT calculations yield a very small value of 0.1 eV for λ_i in the case of the $^1A_g{}^P \otimes {}^1A_g{}^{C_{60}} \rightarrow {}^2B_{2g}{}^{P+} \otimes {}^2T_{1u}{}^{C_{60}-}$ transition;

we expect similar values of λ_i for local-excited states. The intermolecular contribution to λ is equal to the change in electronic polarization that arises as a result of intermolecular geometric relaxation.[28] Unfortunately, there are currently no
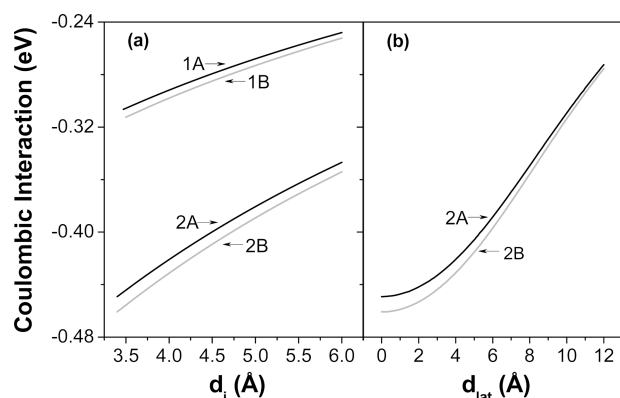
Figure 5. Evolution of the Coulomb energy of the lowest CT state ($^2B_{2g}^{P+} \otimes ^2T_{1u}^{C_{60}-}$) as a function of the intermolecular distance for perpendicular orientations 1A and 1B and parallel orientations 2A and 2B (a) and as a function of lateral displacement for parallel orientations 2A and 2B with $d_i = 3.5$ Å (b).
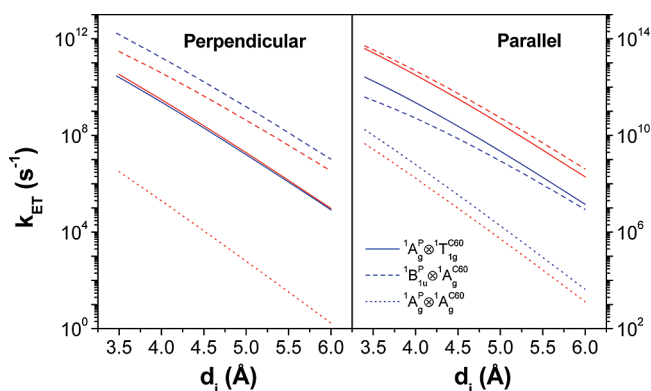

Figure 6. Dependence of the CT rates [from local-excited states $^1A_g^P \otimes ^1T_{1g}^{C_{60}}$ (solid lines) and $^1B_{1u}^P \otimes ^1A_g^{C_{60}}$ (dashed lines) to the CT$_0$ state, $^2B_{2g}^{P+} \otimes ^2T_{1u}^{C_{60}-}$] and CR rates [from the lowest CT state to the ground state, $^2B_{2g}^{P+} \otimes ^2T_{1u}^{C_{60}-} \rightarrow ^1A_g^P \otimes ^1A_g^{C_{60}}$ (dotted lines)] as a function of intermolecular distance. Blue lines refer to orientations 1A and 2A and red lines to orientations 1B and 2B of Figure 1. In the case of orientation 1A, the CR rate is equal to zero.

straightforward models to accurately estimate this coupling for nonpolar systems. Therefore, we assume here a value of 0.5 eV for the overall reorganization energy, λ. This value is similar to that estimated for the CT and CR processes recently investigated in the case of corrole−fullerene dyads in nonpolar solvents.[57]

The calculated CT and CR rates are shown in Figures 6 and 7. Figure 6 highlights that, for typical intermolecular distances of ∼3.5−4.5 Å between adjacent molecules, the electron-transfer rates from local (intramolecular) excited states to the lowest CT state can be very large. These rates can reach ∼10^{10}−10^{12} s^{-1} even in the case of perpendicular configurations of the P/C$_{60}$ complex that do not lead to large electronic couplings; the results indicate that, for such orientations, pentacene-based excitons dissociate at least 10 times faster than fullerene-based excitons. When going from perpendicular to parallel configurations, there occurs a significant increase in the dissociation rate for fullerene-based excitons that comes from an increase in the related electronic coupling and driving force. In the case of electron transfer from the lowest excited state of pentacene, the CT rate
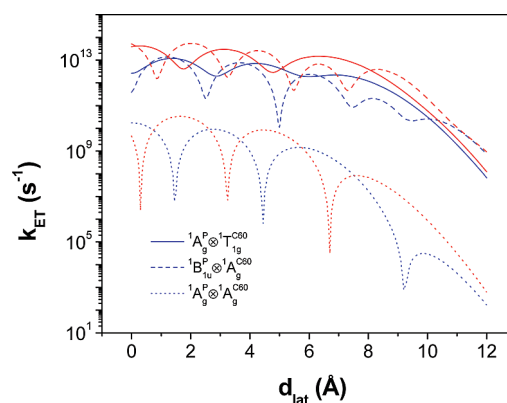
(57) D'Souza, F.; Chitta, R.; Ohkubo, K.; Tasior, M.; Subbaiyan, N. K.; Zandler, M. E.; Rogacki, M. K.; Gryko, D. T.; Fukuzumi, S. *J. Am. Chem. Soc.* **2008**, *130*, 14263–14272.
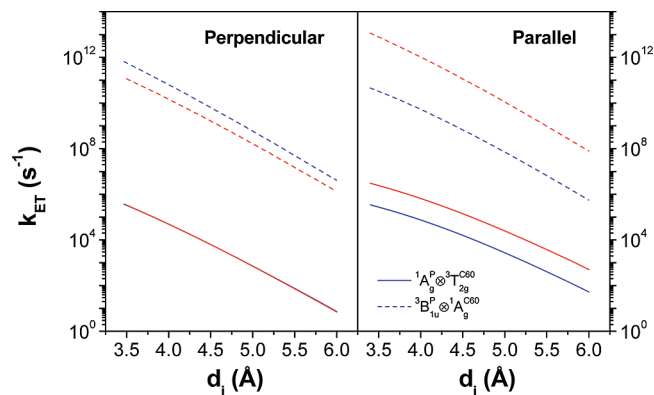
Figure 7. Dependence of the CT rates [from local-excited states $^1A_g^P \otimes ^1T_{1g}^{C_{60}}$ (solid lines) and $^1B_{1u}^P \otimes ^1A_g^{C_{60}}$ (dashed lines) to the lowest CT state, $^2B_{2g}^{P+} \otimes ^2T_{1u}^{C_{60}-}$] and CR rates [from the lowest CT state to the ground state, $^2B_{2g}^{P+} \otimes ^2T_{1u}^{C_{60}-} \rightarrow ^1A_g^P \otimes ^1A_g^{C_{60}}$ (dotted lines)] as a function of lateral displacement for orientations 2A (blue lines) and 2B (red lines) with $d_i = 3.5$ Å.

significantly increases for the "hexagon"-type parallel geometry (2B); for the "edge"-type configuration (2A), the rate is similar to that in the perpendicular orientation (1A).

Following the trend observed for V_{eff}, the electron-transfer rates show an oscillatory dependence as a function of lateral distance. Interestingly, as can be seen from Figure 7, the exciton dissociation rates for lateral displacements (d_{lat}) in the range of ∼0−8 Å consistently remain above 10^{12} s^{-1} for C$_{60}$-based excitons; on the other hand, for pentacene-based excitons, the rates can vary sharply from 10^{12} s^{-1} down to vanishing values. For lateral displacements larger than 11 Å, at which point there is no longer any spatial overlap between C$_{60}$ and pentacene, the CT rates display a monotonic exponential decay as a function of d_{lat}. Thus, our calculations suggest that, irrespective of the geometrical configurations of the P/C$_{60}$ interface, both types of excitons, be they formed on pentacene or on C$_{60}$, are able to dissociate efficiently.

It is also important to discuss the CR rates between the lowest CT state and the ground state. Figures 6 and 7 illustrate that the CR rates can be very large for parallel configurations of the P/C$_{60}$ complex, reaching values over 10^{10} s^{-1}. In the case of "hexagon"-type perpendicular configurations, the CR rates are below 10^7 s^{-1} even for small intermolecular distances. Moreover, in the case of "edge"-type configurations, as a result of the weak electronic interactions, the CR rates become vanishingly small. Very small CR rates are also found for parallel but significantly displaced configurations of the P/C$_{60}$ complex.

A key feature of the CR process is that it can also take place via triplet states. The calculated CR rates from the lowest CT state to local (molecular) triplet states are shown in Figures 8 and 9. Such pathways are especially relevant for perpendicular configurations of the P/C$_{60}$ complex, where a direct transition to the ground state is not efficient.

In the parallel configurations, the CR rates for "hexagon"-type configurations are much larger than those for the "edge"-type configurations, while in the perpendicular orientations these rates are similar (see Figure 8). Figure 9 shows that, in the same way as for electron transfer from the local singlet excited states to the CT state, the CR rates to the local triplet states first display an oscillatory dependence on lateral displacement and then decrease exponentially once the overlap between pentacene and C$_{60}$ vanishes. Our results indicate that the electronic coupling between the CT state and the lowest triplet state of either

Figure 8. Dependence of the CR rates [from the lowest CT state $^2B_{2g}{}^{P+}\otimes^2T_{1u}{}^{C_{60}-}$ to local (molecular) triplet states $^1A_g{}^P\otimes^3T_{2g}{}^{C_{60}}$ (solid lines) and $^3B_{1u}{}^P\otimes^1A_g{}^{C_{60}}$ (dashed lines)] as a function of intermolecular distance. Blue lines refer to orientations 1A and 2A and red lines to orientations 1B and 2B of Figure 1.
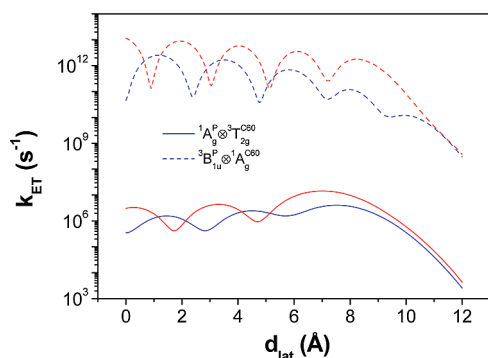

Figure 9. Dependence of the CR rates [from the lowest CT state $^2B_{2g}{}^{P+}\otimes^2T_{1u}{}^{C_{60}-}$ to local-excited triplet states $^1A_g{}^P\otimes^3T_{2g}{}^{C_{60}}$ (solid lines) and $^3B_{1u}{}^P\otimes^1A_g{}^{C_{60}}$ (dashed lines)] as a function of lateral displacement for orientations 2A (blue lines) and 2B (red lines) with $d_i = 3.5$ Å.

pentacene or C$_{60}$ is very much the same as that derived for the corresponding singlet state. However, since the T$_1$ state of C$_{60}$ lies above the lowest CT state (leading to a positive driving force), the CR rate to the T$_1$ state of C$_{60}$ is over 4 orders of magnitude smaller than that of pentacene. The electron-transfer rate from the CT$_0$ state to the triplet state of pentacene is found to be quite fast and comparable to that for exciton dissociation. Since the CT$_0$–pentacene T$_1$ transition first requires a CT$_0$ singlet-to-triplet transition, the overall CR rate via this pathway is obviously limited by the rate of the intersystem crossing process.

To summarize, our results suggest that in the case of bilayer heterojunctions, where pentacene and fullerene molecular pairs

are expected to be mainly in perpendicular or displaced-parallel orientations, the CR processes from the CT state will play a less significant role than in the case of P/C$_{60}$ bulk heterojunctions, where a substantial number of P/C$_{60}$ complexes should be found in parallel configurations. In the latter case, the CR process could therefore compete efficiently with the dissociation of the CT states into mobile charge carriers and constitute an adverse factor limiting device performance.

4. Conclusions

We have investigated the impact of the intermolecular geometry on exciton-dissociation and charge-recombination processes for pentacene/C$_{60}$ complex. We have evaluated the electronic couplings and the CT and CR rates for several geometrical configurations of the complex that are relevant to P/C$_{60}$ bilayer and bulk heterojunctions.

The results of our calculations suggest that, irrespective of the intermolecular orientations within the complex, both pentacene-based and C$_{60}$-based excitons are able to dissociate efficiently. We also found that, in the case of parallel configurations, the decay of the CT state is very fast and could compete with the dissociation process of the CT state into mobile charge carriers. Since a more substantial number of P/C$_{60}$ complexes in parallel configurations can be expected in bulk heterojunctions, our results imply that the performance of P/C$_{60}$ OPV devices based on such an interfacial structure can suffer more considerably from CR processes than devices based on bilayer heterojunctions.

Supporting Information Available: Electronic couplings between the ground state or the local excited states and the lowest CT state (CT$_0$) for the model orientations (Table S1); electronic couplings between the ground state or the local excited states and the lowest CT excited states (CT$_1$ and CT$_2$) for various intermolecular configurations (Figures S1–S4); complete ref 32; and DFT-optimized neutral and ionic geometries and energies for pentacene and C$_{60}$ (Tables S2 and S3). This information is available free of charge via the Internet at http://pubs.acs.org.

JA905975W